Water Air Soil Pollut (2011) 216:3–19
DOI 10.1007/s11270-010-0510-1

Characterization of AMD Pollution in the River Tinto (SW Spain). Geochemical Comparison Between Generating Source and Receiving Environment

Maria Luisa de la Torre · Jose Antonio Grande · Jorge Graiño · Tamara Gómez · Juan Carlos Cerón

Received: 16 March 2010 / Accepted: 2 June 2010 / Published online: 18 June 2010

Abstract With the aim of obtaining precise knowledge of the spatial–temporal behavior of the chemistry of the river Tinto, both in the area of the headwaters, close to the point at which the acid mine drainage (AMD) pollution is carried into this river, and in the area before tidal influence, daily sampling was carried out from the end of October 2007 to the beginning of June 2008. In addition to pH, conductivity, and redox potential, sulfates, As, Cd, Fe, Cu, Zn, and Mn were determined for each sample. By studying the results obtained from the statistical processing applied, it can be deduced, first and foremost, that the river Tinto is a watercourse which is highly polluted by acid mine drainage throughout its length. It can also be determined that the order of abundance of the polluting elements, in terms of the concentration of the various parameters in milligrams per liter, follows the pattern, both in the generating source and the receiving environment: SO_4 > Fe > Cu > Zn > Mn > Cd > As. The concentration values for As carried into the river in the generating source, with average values of 640 μg l^{-1} and with a maximum of 1,540 μg l^{-1} (ten times greater than the maximum found in the receiving environment), far exceed 10 μg l^{-1}, the value established by the EU as the maximum permissible concentration in drinking water, as a consequence of the high eco-toxicity of this element. Specifically, in the correlation matrix, no correlation was found between the variables for both points. It can only be made out in the cross-correlation function graphs through low correlation, prior to time t=0, that pollution in the generating source leads to pollution in the receiving environment.

Keywords Tinto River · Heavy metals · Arsenic · Acid mine drainage · Iberian pyrite belt · pH · Conductivity · Sulfates

M. L. de la Torre (✉) · J. A. Grande · J. Graiño · T. Gómez
Grupo de Geología Costera y Recursos Hídricos. Escuela Politécnica Superior, Universidad de Huelva,
Ctra. Palos Fra. s/n,
21819 Palos de la Frontera, Huelva, Spain
e-mail: mltorre@uhu.es

J. C. Cerón
Grupo de Geomorfología ambiental y Recursos Hídricos. Facultad de Ciencias Experimentales,
Universidad de Huelva,
Avda. 3 de marzo s/n,
21007 Huelva, Spain
e-mail: ceron@uhu.es

1 Introduction

Acid mine drainage (AMD) is polluted water that normally contains high levels of iron, copper, zinc, aluminum, and sulfuric acid. Contaminated waters are often orange or yellowish-orange in color, indicating high levels of iron, and may also smell like rotten eggs (hydrogen sulfide; Cheng et al. 2008).

Weathering of sulfide-rich mining waste causes AMD. These effluents are characterized by low pH and contain significant quantities of sulfates, metal, and

metalloids, including As. AMD generation can persist hundreds of years after the mine closed jeopardizing water resources and causing deleterious effects on aquatic life (Demchack et al. 2004 in Casiot et al. 2009).

Although the overriding chemical mechanism of AMD has now been reasonably understood, accurate assessment or prediction of its ecological impacts is still difficult due to the complexity of the processes involved. Environmental factors such as climatic, hydrological, geomorphic, geological, and biological conditions could significantly affect the rate of sulfide-derived acid generation and the mode of transport and transformation of sulfide oxidation products (Lin et al. 2007).

AMD is the principal problem pyrite mining exploitations have to face, not only due their ecological effects, but because once it has appeared, it is virtually impossible to correct, since processing using current technology costs millions of dollars and might continue for many centuries (EMCBC 1996).

The Iberian Pyrite Belt is located in the south-west of the Iberian Peninsula (Fig. 1), forming a metallogenic province 230-km long and 30-km wide. Almost all the deposits in this belt and, in particular, the Riotinto mining deposit, approximately 5 km^2 in area and which is one of the largest deposits of massive sulfur in the world, are to be found in the province of Huelva. Pyrite, with a greater or lesser proportion of copper, is the principal mineral and reveals an average content of 46–49% of sulfur, 40–45% of iron, 0.6–1% of copper, 0.5–1.5% of lead, 1–3% of zinc, and 0.1–0.6% of arsenic and other metals (Ortiz 2003).

The Iberian Pyrite Belt contains a number of giant and super-giant Paleozoic massive sulfur deposits, the largest in the world, according to Sáez et al. (1999). These authors calculate the reserves at in excess of 1,500 Mt, distributed over eight super-giant deposits (>100 Mt) and an undetermined number of other smaller deposits, jointly associated with stockwork- and footwall-alteration-halo-type mineralizations. The massive sulfur bodies contain pyrite, with which are associated to sphalerite, galene, and chalcopyrite and many minor phases (Sáez et al. 1999). These deposits have been exploited for more than 2,000 years with many extensive abandoned mining workings left as the remains of this activity, as well as several million tons of ancient slag of different composition (Pinedo Vara 1963).

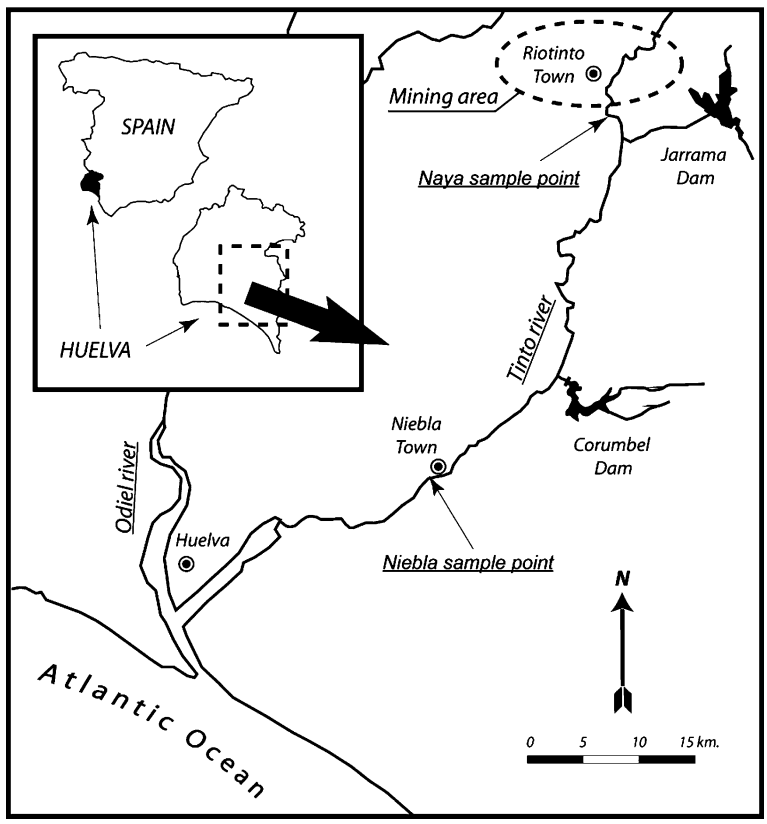

Fig. 1 Location map

The Riotinto mining field has been exploited for more than 5,000 years (Ortiz 2003). The metallogenic importance of the field has caused the Tartessians, Phoenicians, Romans, Arabs, and Spanish to pass through its mines in search of its minerals. At present, none of the mining exploitations remains active; however, dispersed throughout the geography of the area, abandoned exploitations still continue to produce serious pollution after many decades of inactivity. Internal upwellings, leachates from slag heaps and the rinse water from all kinds of pyrite waste, continue to convey acidity, sulfates, and heavy metals into the rivers Tinto and Odiel, pollutants which these transport, in turn, to the Huelva estuary and the littoral zone into which the waters flow (Sáinz et al. 2002).

The river Tinto rises in Peña del Hierro, a mine located in the Riotinto complex of mines, on a deposit that includes massive sulfides and their gossanized remains which resemble some iron and sulfur minerals found on Mars (Stoker et al. 2008). The Tinto River is a small watercourse (approx. 100-km along) which constitutes a 25-km-long incised estuary in the confluence with the Odiel River in the south-western Spain coast (Ruiz et al. 2008).

There are many studies which have been carried out on the environment of the river Tinto, some relating to the chemistry of its waters, such as those by Grande et al. (2003a, b, 2005a, b), Aroba et al. (2007), Jiménez et al. (2009), de la Torre et al. (2009), Olías et al. (2004), Vicente-Martorell et al. (2009), Sarmiento et al. (2009a, b), Egal et al. (2008), Cánovas et al. (2008), Sobron et al. (2007), Nieto et al. (2007), Sánchez-Rodas et al. (2005), and Sáinz et al. (2002, 2003, 2004, 2005); its sediments, such as those by Ruiz et al. (2008), Borrego et al. (2002), Morales et al. (2008); and even the area in the vicinity of the source of the river Tinto as pilot experience of the conditions on the surface of Mars, such as those works by Stoker et al. (2008), Amils (2006), or Fernández-Remolar et al. (2004), among others.

However, during the review of previous research prior to starting this study, no works were found focusing on comparison of the geochemical behavior of the river Tinto in the generating source and the receiving environment. This is precisely the aim of this work, which attempts to obtain exact knowledge of the spatial–temporal behavior of the chemistry of the river Tinto, both in the area of the headwaters, close to the point at which the AMD pollution is carried into this river, and in the area before tidal influence.

2 Materials and Methods

2.1 Sampling Sites

With the aim of achieving the predetermined objective, it was established that a daily sample of water would be taken at the head of the river Tinto and another as close as possible to the mouth, before the point where tidal influence begins.

At the headwaters, the sample-taking was planned at a point of confluence of all the waters originating from drainage of the mines and the slag heaps which make up the Riotinto Mines mining complex before they flow into the basin of the river Tinto, as another part of the water flows into the basin of the river Odiel. For this reason, Naya was established as the sampling site for the generating source (see Fig. 1). Waters from the river Tinto reach this site from their source in Peña del Hierro, after passing through Marismillas dam, following which it is joined by a stream from Cerro Colorado. Downstream, waters also arrive from tunnel no. 16 in the Atalaya open pit mine and before the Naya sampling site.

Downriver, the sampling site is Niebla (Fig. 1), where tidal influence does not reach (Grande et al. 2003).

Between the Naya and Niebla sites, there are no more acid mine drainage discharges into the river Tinto. The only tributaries are the Corumbel and Jarrama, whose waters are clean, since they do not pass through any mining areas. In addition, both tributaries are regulated by dams which form reservoirs whose waters are used for irrigation and so their contribution to the river Tinto is practically nil.

A water contribution which must not be forgotten is rainwater. Data for rain were obtained from the Spanish State Meteorological Agency, part of the Spanish Ministry for the Environment.

2.2 Sample-Taking and Analysis

Sample-taking at the sites described took place on a daily basis, from the end of October 2007 until the beginning of June 2008.

Two samples were taken in 100-ml polyethylene containers at each site. To one of the samples, 1%

concentration nitric acid was added, which allowed us to keep the pH below 2, a very important factor in the determination of heavy metals because it prevents their precipitation. The other sample was kept unacidulated for the subsequent sulfate analysis. At this point, pH and conductivity were measured in the field using a CRISON MM40 portable multimeter and the redox potential using an OAKTON EUTECH waterproof ORPTestr 10. The samples were placed in an icebox and transported to the laboratory for the analyses to be performed.

In addition to pH, conductivity, and redox potential, sulfates, As, Cd, Fe, Cu, Zn, and Mn were determined for each sample.

The procedure used to analyze each parameter was as follows:

Preliminary processing of the sample consisted of filtering using 0.45-μm cellulose nitrate filters (Sartorious 11406-47-ACN). All reagents used were of analytical grade or higher, from Merck or Panreac. Standards certified by A. A. Panreac were used. The ultra-pure water used in all the analyses was produced by a Milli-Q system.

Measurement of sulfates dissolved in the water was performed using a MACHEREY-NAGEL PF-11 photometer.

For the analysis of heavy metals (Fe, Cu, Mn, and Zn), a Perkin Elmer AAnalyst 800 Spectrometry system was used. The technique employed was atomic absorption using an air–acetylene flame, with hollow cathode lamps as a source of energy. For Cd analysis, the technique used was electrothermal atomic absorption spectrometry, with the AAnalyst 800 system's graphite furnace equipped with Zeeman-effect background correction and an electron discharge lamp. Determination of As required a Perkin Elmer Fias 100 flow injection system.

2.3 Statistical Analysis

The data from measurement of pH, conductivity, and redox potential in the field, as well as from analyses of sulfates, Fe, Cu, Zn, Mn, As, and Cd in the laboratory, were entered into a data matrix which was subsequently submitted, first of all to a study of the statistical summary, and then to multivariate analysis by studying the correlation matrix and temporal evolution, autocorrelation, cross-correlation, and cluster graphs. All this was performed using Statgraphics Centurion XV statistics package.

Correlation matrix Each box shows Pearson's R correlation coefficient, which ranges between 1 and –1 for each pair of variables.

Time series analysis This studies the evolution of a given magnitude over time. In this case, the parameters considered are precipitation and the variations it induces in the chemical composition of the water to determine possible relationships between both.

Autocorrelation function In some cases, it is interesting to correlate the values for a variable x at given times with those corresponding to x at previous times in order to know the system inertia. This function measures the existing correlation between the values taken by the variable for an instant t and the instant $t+k$, with k being the delay or time between one observation and the next (Bisquerra 1989).

Cross-correlation function This function estimates the correlation between a time series at a time t and a second series at an instant $t+k$ as the function of delay or differential time k. It is particularly useful if two series are related to each other, and if they are, to determine whether one leads to the other.

The term "cluster analysis" is used to define a series of techniques, basically algorithms, whose object is to look for similar groups of items or variables which are grouped together in clusters. When applied to a set of variables, cluster analysis orders and classifies them in the most homogenous groups possible based on the similarity of the variables themselves. Both cluster and discriminatory analyses are used to classify individuals into categories (Bisquerra 1989 in Grande et al. 2003).

3 Results

3.1 Statistical Summary

Tables 1 and 2 show the statistical summary of the parameters analyzed in both the generating source (Naya) and the receiving environment (Niebla).

In establishing a comparison between both sites, it is worth pointing out that pH does not reveal very disparate values, with the average value in Naya at 2.5 and in Niebla 2.53. The minimum pH value is similar at both sites, although the maximum value, in

Table 1 Statistical summary of the parameters analyzed in the generating source (Naya)

		Mean	Median	Standard deviation	Variance	Minimum	Maximum	Lower quartile	Upper quartile
pH Nay		2.5	2.5	0.13	0.018	1.82	2.7	2.5	2.6
Cond Nay	$\mu S\ cm^{-1}$	12.76	12.78	1.91	3.62	2. 3	17.95	12.1	13.75
Pot Rdx Nay	mV	433.01	432.5	12.53	157.10	405	468	424.5	440
As Nay	$mg\ l^{-1}$	0.64	0.78	280.5	78,686.90	0.23	1.54	0.51	0.90
Cd Nay	$mg\ l^{-1}$	2	2.22	463.13	214,489	1.02	2.86	1.74	2.35
Cu Nay	$mg\ l^{-1}$	329.83	335.2	105.87	11,209.4	84.42	643.3	274.01	401.75
Fe Nay	$mg\ l^{-1}$	2,352.77	2,540.5	487.13	237,297	1,129	3,100	2,049	2,821
Zn Nay	$mg\ l^{-1}$	494.55	517.90	184.52	34,046.6	50.9	1,494	422.45	612.10
Mn Nay	$mg\ l^{-1}$	141.55	146.72	31.79	1,011.13	51.6	219.1	123.62	166.40
SO_4 Nay	$mg\ l^{-1}$	8,256.8	9,500	3,628.52	1.3E7	1,040	16,000	6,721.5	12,250

In all cases, it is calculated for a total of 108 pieces of data

the case of Niebla, rises to 3.4, while in Naya, it only reaches 2.70. In both cases pH variance is low.

In terms of conductivity, it can be seen that the average value for this parameter in Niebla is 175 times higher than the average value in Naya, while it can be pointed out that the variance, in the case of Niebla, is 180,707 times higher than the value calculated for the generating source. In addition, in Niebla the maximum value for conductivity reaches close to 5,500 μS/cm, while in Naya, it only reaches 17.95 μS/cm. It is worth pointing out that just as reflected in Grande et al. (2003), tidal influence does not reach the Niebla sampling site.

The redox potential has an average value of 433.01 mV in Naya and 845 mV in Niebla. It can be especially highlighted that the variance value in Niebla rises to 425,754 while in Naya, it reaches a value close to 160.

As for arsenic, it is important to point out an average value of 0.64 $mg\ l^{-1}$ in the generating source (Naya), with the maximum value rising to 1.54 $mg\ l^{-1}$. In addition, it can be seen that 75% of the data have a value greater than 0.9 $mg\ l^{-1}$. When the water reaches Niebla, the average As value has fallen to 0.042 $mg\ l^{-1}$, with the variance of this parameter reduced 1,300 times.

In the same way, the average Cd concentration goes from a value of 2 $mg\ l^{-1}$, at the headwaters, falling to 0.1 $mg\ l^{-1}$ in Niebla.

The remaining parameters, the result of AMD pollution, also follow similar behavior, with their average concentration values falling from the generating source

Table 2 Statistical summary of the parameters analyzed in the receiving environment (Niebla)

		Mean	Median	Standard deviation	Variance	Minimum	Maximum	Lower quartile	Upper quartile
pH Nie		2.53	2.62	0.37	0.13	1.31	3.4	2.36	2.85
Cond Nie	$\mu S\ cm^{-1}$	2,239	2,376.50	809.91	655,969	757.00	5,493.33	1,918.00	2,722.50
Pot Rdx Nie	mV	844.96	596.00	652.50	425,754	451.50	3,493.00	552.50	1,550.00
As Nie	$mg\ l^{-1}$	0.042	0.044	26.93	725.33	0.004	0.142	0.031	0.072
Cd Nie	$mg\ l^{-1}$	0.094	0.099	43.50	1,891.78	0.024	0.247	0.068	0.132
Cu Nie	$mg\ l^{-1}$	23.84	25.32	14.89	221.65	3.89	74.13	19.4	30.71
Fe Nie	$mg\ l^{-1}$	316.43	361.10	365.40	133,523	46.30	1,485.00	155.30	555.80
Zn Nie	$mg\ l^{-1}$	20.26	19.62	17.47	305.17	3.42	77.51	14.02	30.54
Mn Nie	$mg\ l^{-1}$	10.36	9.99	6.48	42.11	3.76	32.37	7.78	12.68
SO_4 Nie	$mg\ l^{-1}$	370.54	396.00	150.26	22,577.80	123.00	776.00	288.00	494.00

In all cases, it is calculated for a total of 108 pieces of data

Table 3 Pearson correlation matrix for the parameters analyzed in Naya and Niebla

	pH Nay	Cond Nay	Pot rdx Nay	As Nay	Cd Nay	Cu Nay	Fe Nay	Zn Nay	Mn Nay	SO_4 Nay	pH nie	Cond nie	Pot rdx nie	As nie	Cd nie	Cu Nie	Fe Nie	Zn nie	Mn nie	SO_4 nie	Rain
pH Nay																					
Cond Nay	−0.1010																				
	0.3408																				
Pot rdx Nay	0.2907	−0.1141																			
	0.0052	0.2815																			
As Nay	−0.0274	0.2364	−0.0950																		
	0.7968	0.0241	0.3706																		
Cd Nay	0.1865	−0.1755	−0.0924	0.1113																	
	0.0767	0.0962	0.3835	0.2938																	
Cu Nay	0.0v	0.1240	−0.0293	0.1268	0.0155																
	0.7733	0.2417	0.7824	0.2312	0.8843																
Fe Nay	−0.0258	−0.1794	−0.2055	0.0057	0.2284	0.0555															
	0.8081	0.0888	0.0506	0.9571	0.0294	0.6011															
Zn Nay	0.1484	0.0391	−0.0423	0.1985	0.4695	0.2163	0.1469														
	0.1605	0.7131	0.6908	0.0592	0.0000	0.0395	0.1646														
Mn Nay	0.1598	0.1341	−0.0488	0.2712	0.3837	0.2975	0.2174	0.5558													
	0.1303	0.2050	0.6463	0.0093	0.0002	0.0042	0.0384	0.0000													
SO_4 Nay	−0.0865	0.1412	−0.1497	0.2791	0.3035	0.1510	0.1488	0.3638	0.3213												
	0.4151	0.1820	0.1566	0.0074	0.0035	0.1531	0.1593	0.0004	0.0019												
pH Nie	0.1732	−0.0475	−0.0965	−0.0345	0.0434	0.0494	−0.1017	0.0358	0.1708	0.0743											
	0.1006	0.6547	0.3630	0.7453	0.6827	0.6420	0.3373	0.7360	0.1055	0.4841											
Cond nie	0.0714	−0.0780	0.2294	−0.3376	−0.1569	−0.0890	−0.1346	−0.1614	−0.1410	−0.2302	−0.3625										
	0.5014	0.4621	0.0287	0.0011	0.1375	0.4017	0.2032	0.1263	0.1825	0.0281	0.0004										
Pot rdx nie	−0.0491	−0.1895	−0.1734	−0.0250	0.1466	0.1584	0.0486	0.1171	0.0260	0.0876	0.6176	−0.5070									
	0.6438	0.0719	0.1003	0.8137	0.1655	0.1338	0.6474	0.2689	0.8069	0.4088	0.0000	0.0000									
As nie	−0.1225	0.1791	0.1270	−0.1326	−0.3434	−0.0774	−0.05v	−0.4214	−0.2636	−0.3009	−0.0002	0.1825	−0.0753								
	0.2474	0.0894	0.2303	0.2102	0.0009	0.4656	0.6145	0.0000	0.0116	0.0038	0.9982	0.0833	0.4784								
Cd nie	0.1412	−0.1193	0.2495	−0.2850	−0.0347	−0.1951	−0.1899	−0.1377	−0.1464	−0.2123	−0.0923	0.5119	−0.1172	0.2718							
	0.1820	0.2599	0.0171	0.0062	0.7437	0.0639	0.0713	0.1931	0.1663	0.0434	0.3844	0.0000	0.2684	0.0092							
Cu nie	0.0024	−0.3786	−0.0405	−0.0080	0.0109	0.0912	0.0731	−0.0710	−0.0400	−0.0679	0.0694	0.1572	0.0906	−0.0936	0.2384						
	0.9823	0.0002	0.7033	0.9401	0.9182	0.3902	0.4911	0.5035	0.7065	0.5227	0.5135	0.1368	0.3931	0.3774	0.0239						
Fe nie	−0.0997	−0.2968	−0.1829	0.1753	0.1170	0.2327	0.1872	0.1764	0.1275	0.0774	0.1686	−0.2211	0.3423	−0.3588	−0.2065	0.6618					
	0.3472	0.0043	0.0827	0.0966	0.2695	0.0254	0.0756	0.0945	0.2285	0.4660	0.1102	0.0352	0.0009	0.0005	0.0494	0.0000					
Zn nie	0.0640	−0.3914	−0.0412	−0.0113	0.0969	0.1042	0.1024	0.0013	0.0357	−0.0650	0.0707	0.1279	0.0986	−0.0691	0.2153	0.8962	0.6686				
	0.5465	0.0001	0.6982	0.9154	0.3609	0.3255	0.3340	0.9900	0.7366	0.5407	0.5054	0.2269	0.3526	0.5152	0.0404	0.0000	0.0000				
Mn Nie	−0.0249	−0.3581	−0.1347	−0.0547	0.1071	0.1898	0.0481	0.0455	0.1212	0.0221	0.1347	0.1628	0.1409	−0.0776	0.1561	0.7945	0.5698	0.8212			
	0.7429	0.0005	0.2029	0.6067	0.3125	0.0716	0.6509	0.6684	0.2523	0.8351	0.2031	0.1230	0.1827	0.4644	0.1394	0.0000	0.0000	0.0000			

SO_4 nie	0.0099	−0.0753	−0.0747	−0.1769	−0.0373	−0.2285	−0.0051	−0.1388	−0.1470	−0.3868	0.0826	−0.0418	0.1451	0.1077	0.1403	0.0588	−0.0826	0.1689	0.0359	
	0.9260	0.4782	0.4817	0.0934	0.7256	0.0294	0.9620	0.1895	0.1645	0.0002	0.4363	0.6937	0.1699	0.3096	0.1859	0.5801	0.4366	0.1094	0.7353	
Rain	−0.0920	−0.2458	−0.0581	−0.2575	−0.1187	−0.2240	−0.0580	−0.0676	0.0245	−0.1543	0.1144	0.1620	0.1178	−0.0494	−0.0530	−0.0161	0.2019	0.0372	0.0731	0.0200
	0.3858	0.0188	0.5845		0.2623	0.0328	0.5850	0.5243	0.8176	0.1442	0.2802	0.1250	0.2661	0.6406	0.6181	0.8794	0.0550	0.7264	0.4910	0.8504

In each parameter is indicated, first row, the correlation coefficient between each pair of variables and, second row, the statistical significance of the estimated correlations (values less than 0.05 indicate a level of confidence of 95%)

to the receiving environment. Specifically, Fe goes from an average value of 2,352.77 to 317 mg l^{-1}, Cu from 329.83 to 24 mg l^{-1}, Zn falls from 494.55 to 20 mg l^{-1}, and Mn goes from around 140 to some 10 mg l^{-1}.

Sulfate, a characteristic parameter for this type of pollution from pyrite mines, deserves special consideration. In Table 1, it can be seen that the average concentration of this parameter rises to some 8,200 mg l^{-1}, reaching a maximum value of 16,000 mg l^{-1} in the generating source. In addition, at this sampling site, the variance shoots up to values of 1.3×10^{7}. When the water reaches Niebla, the average sulfate concentration values have fallen to 370.5 mg l^{-1}, and the variance, just as what happened with the pH and unlike the metals, is clearly lower (575 times) in the receiving environment.

3.2 Correlation Matrix

Table 3 shows the resulting correlation matrix applied to the two sampling sites.

At first sight, the first thing to notice is the lack of correlation between the same parameters, between the generating source (Naya) and the receiving environment (Niebla).

On the other hand, we find the following correlations, higher than a Pearson coefficient of 0.5:

A correlation is only observed between Zn and Mn in Naya, with a Pearson coefficient of 0.5558.

As for Niebla, the following correlations are established: pH and redox potential (0.6), conductivity and redox potential (−0.5), conductivity and cadmium (0.51), copper with Fe (0.66), Zn (0.89), and Mn (0.79); Fe with Zn (0.668) and Mn (0.57), as well as Zn with Mn (0.82).

Rain does not correlate with any other parameter.

3.3 Temporal Evolution Graphs

Temporal evolution graphs have been plotted for each parameter (Fig. 2a–k), establishing a comparison over time, and in the evolution of the chemistry at each sampling point, with the rain. By studying the resulting graphs, the following can be deduced:

In Naya (Fig. 2b), pH does not suffer very pronounced changes throughout the period of study. Indeed, after an episode of heavy rain, no substantial changes in pH are detected which might lead us to think that rain substantially affects this parameter in the

generating source. Slight increases in pH are only observed after rain, followed by moderate decreases a few days later. However, in Niebla an evolution can indeed be deduced over time in the pH values with more pronounced fluctuations, always staying between a minimum of 1.3 and a maximum of 3.4, i.e., always very acidic pH. At this site, it can indeed be discerned that rain has a greater influence. It can be seen that heavy rain on day 4 corresponds to a rise in pH 1 or 2 days later and then a fall again. This very behavior can be seen on day 85. In addition, from day 65 onwards, a general increase in pH can be observed in Niebla.

In terms of conductivity (Fig. 2c), it can be seen, at the two sampling sites, that at the beginning of the hydrological year, heavy rain produces an immediate response of a sharp drop in conductivity. On the other hand, a staggered, inverse evolution can be observed at both sites, i.e., in Naya, after the first rains, and following a large drop in the conductivity value, a large increase is produced in the latter followed by a gradual decrease over the course of approximately 1 month, and then another step is produced, again consisting of a sharp rise and gradual fall that spread out over a period of time. This same phenomenon, but inverted, is seen in Niebla; the sharp rise in conductivity in Naya corresponds in time with a sharp fall in Niebla followed, in this case, by a gradual increase that spreads out over a similar period. Then at the same time, a new step, which is inverse to that at the site in the generating source, begins in Naya.

The redox potential in Naya (Fig. 2d) is found to have lower values than those measured in Niebla throughout

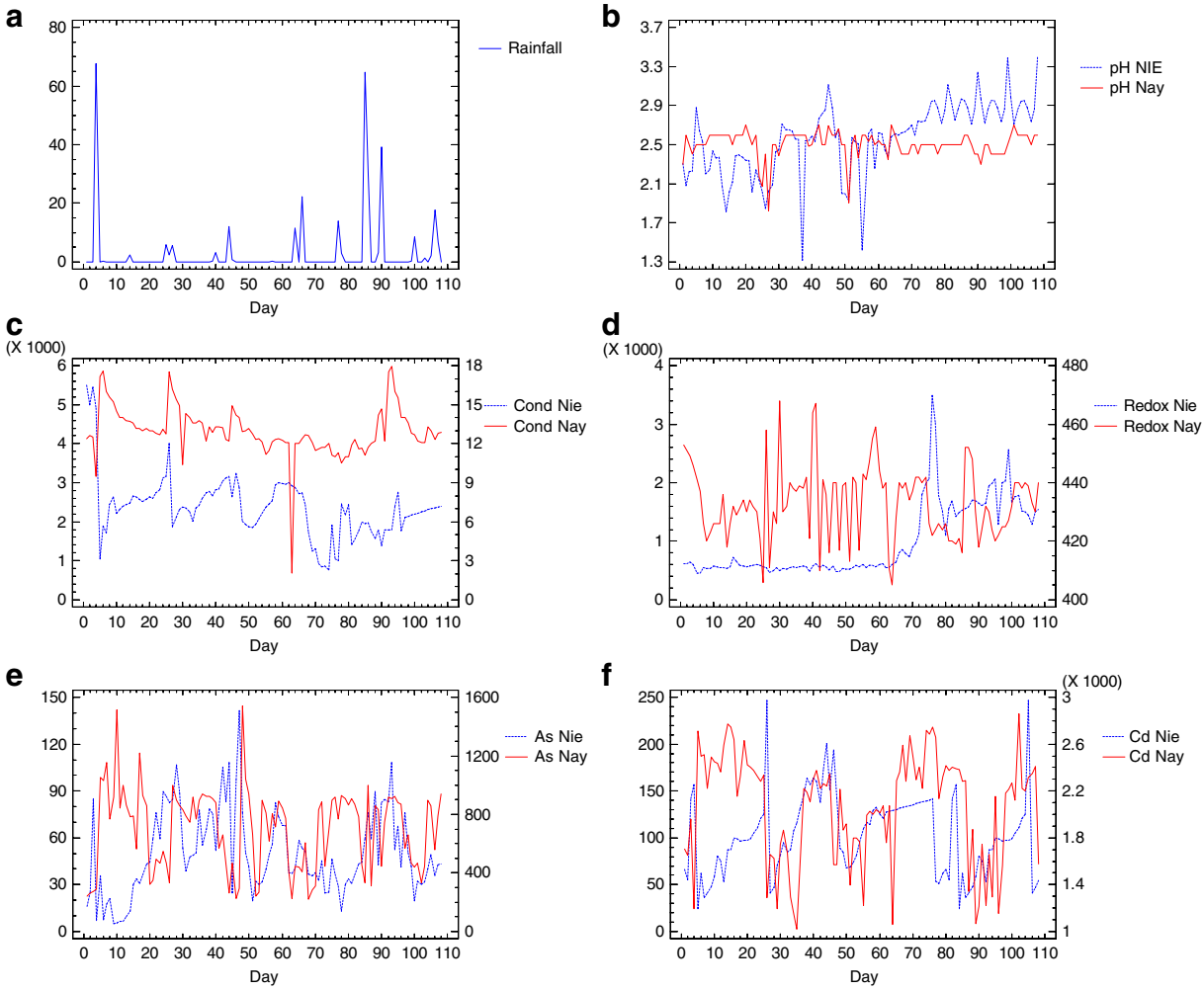

Fig. 2 Temporal evolution graphs

the sampling period. An increase in redox potential is observed in the receiving environment just as in the case of pH, from day 65 until the end of the period of study.

No harmonious evolution in As is noticed over time (Fig. 2e) but rather at both sites, sawtooth evolution in concentration is detected over time, with continual rises and falls in the concentration of this element. Throughout the period of study, the As concentration in Naya is found to be much higher than in Niebla. There is no relationship observed in the evolution of As at both sampling sites.

As for cadmium (Fig. 2f), staggered evolution is detected in Niebla, coinciding in form and in time with that observed for conductivity at this same point. In Naya (the generating source), the temporal evolution in Cd concentration is a sequence of rises and falls which apparently follows no pattern with rain or other parameters.

In the temporal evolution graph for Zn (Fig. 2g), an initial fall is detected after the first rains, followed by a rise in concentration, both in the generating source and in the receiving environment. In terms of general temporal evolution, similar behavior is observed at both sites, with the concentration of Zn at each point always higher in the generating source than in the receiving environment. Mn (Fig. 2j) and Cu (Fig. 2h) follow a similar pattern to Zn.

Iron (Fig. 2i) also describes a sawtooth evolution with more pronounced continual rises and falls in concentra-

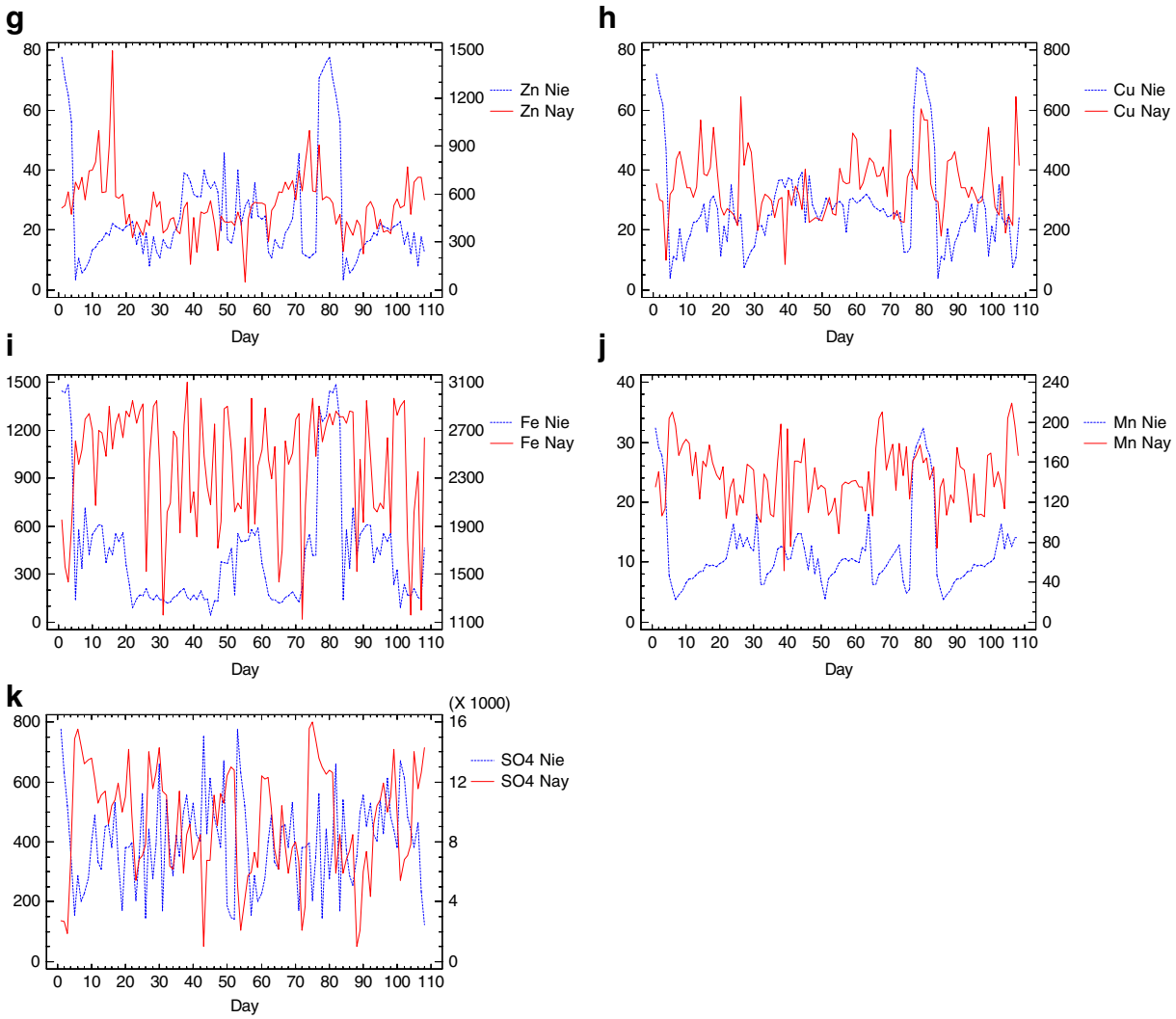

Fig. 2 (continued)

tion values in the generating source, with concentration in Niebla at all times below that determined in Naya.

In the graphic obtained for sulfates (Fig. 2k), it is observed that, contrary to what was described for other parameters, after the first rains, there is no initial decrease in concentration in the generating source but rather an immediate rise is detected in this value which continues an evolution of continual rises and falls in concentration through time without any general evolutionary trend being observed. In the receiving environment, a fall in sulfate concentration is indeed produced after the first rains, and the subsequent evolution is similar to the generating source, but the concentration value is always lower in Niebla.

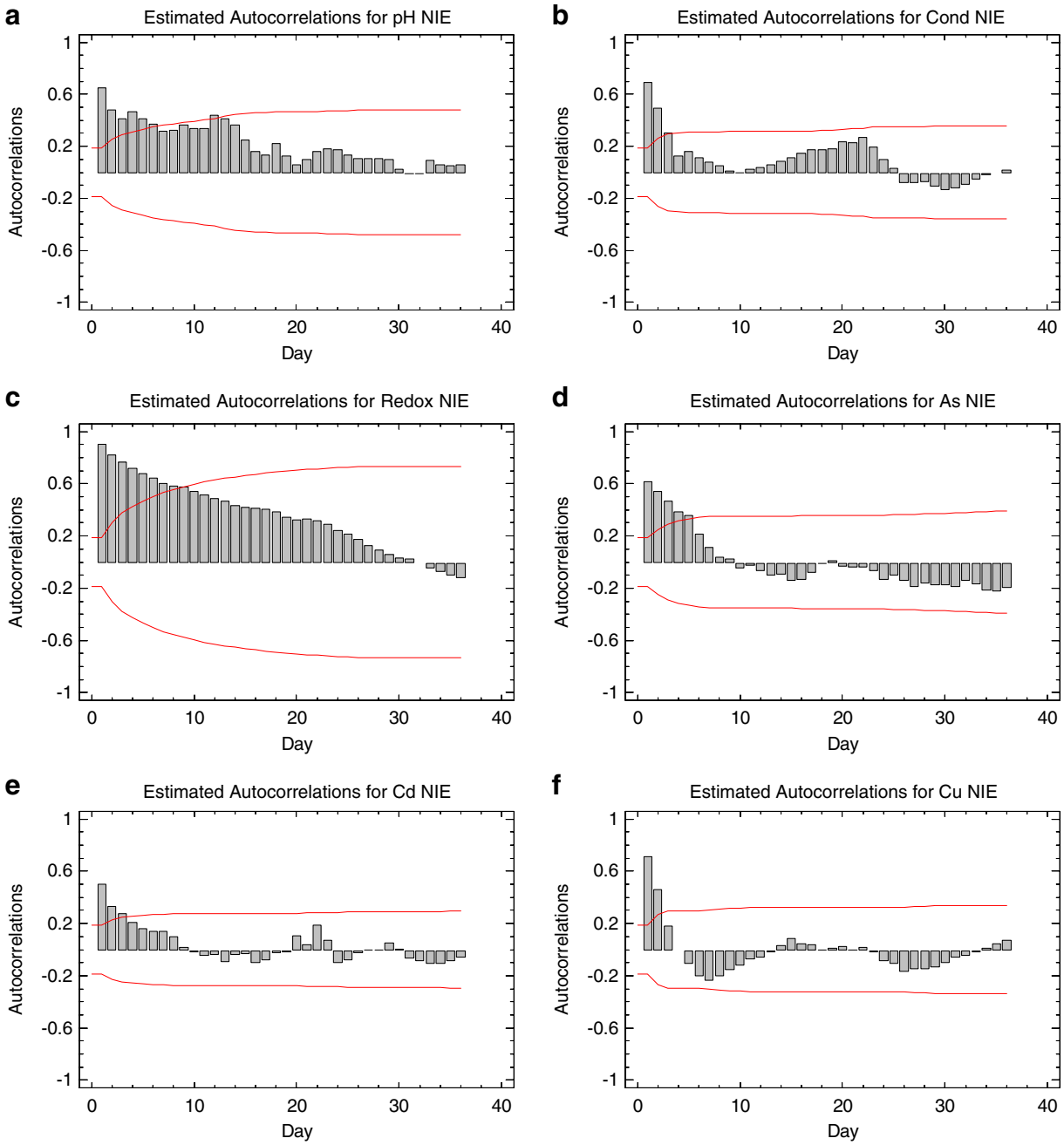

Fig. 3 Graphs showing estimated autocorrelations for each parameter

3.4 Autocorrelations

The autocorrelation function applied to the series studied shows the value for correlations between each variable on 1 day and the same variable on the previous days. The graph (Fig. 3a–t) contains vertical bars that represent the coefficient for each day and a pair of dotted lines at a distance from the baseline that are a multiple of the standard error for each day. For pH we can see that in Naya (Fig. 3k), there are three

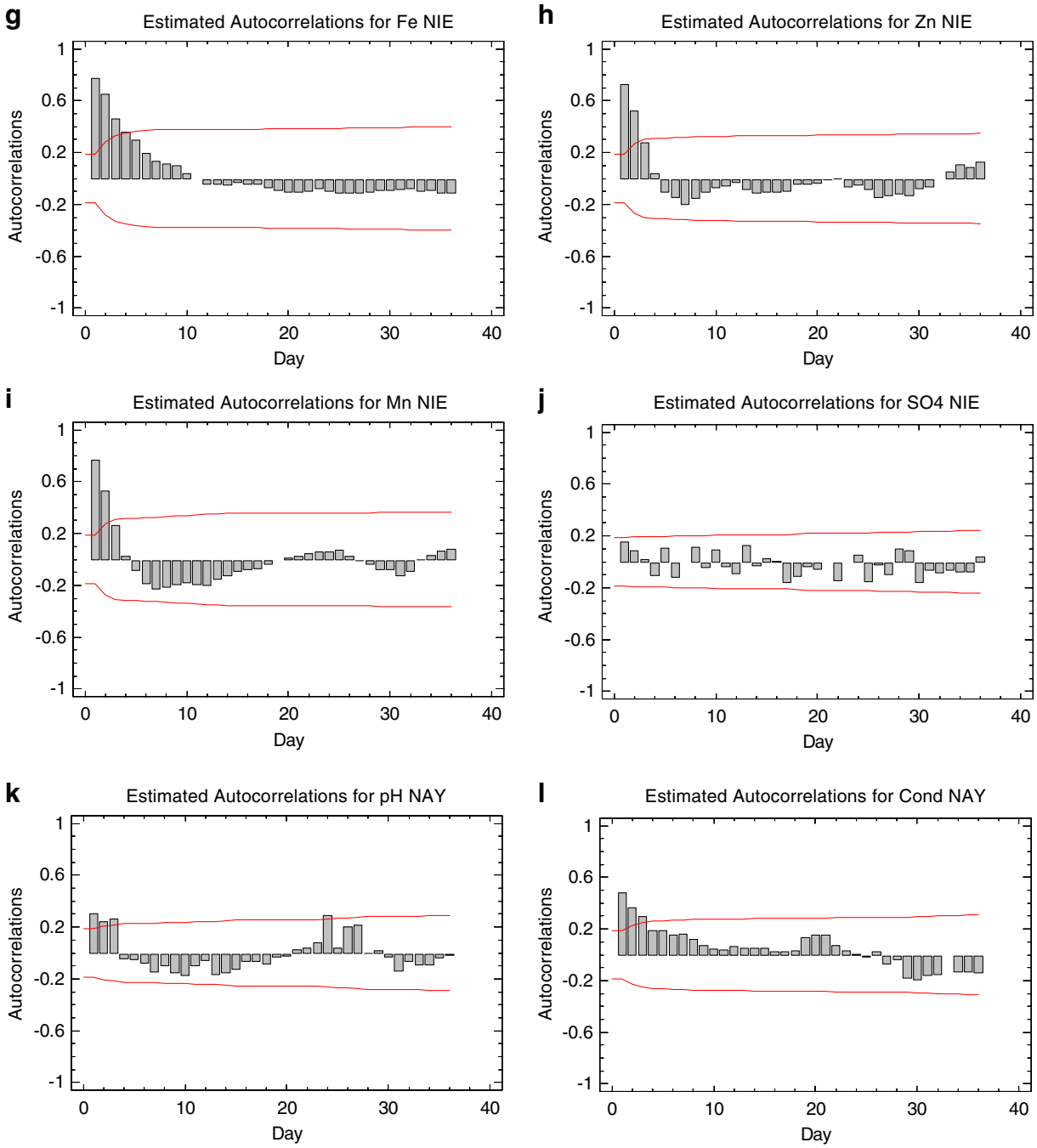

Fig. 3 (continued)

values above the point line, which means they are significantly different from zero, implying the existence of a 3-day memory for the system. That is, pH correlates positively with values from up to four previous days, and from that moment on, the system does not remember. In the case of the Niebla (Fig. 3a), this value is 5.

A similar 3-day memory is observed for conductivity in graphs corresponding to the generating source and receiving environment (Fig. 3b, l).

It is worth pointing out the sizeable difference between the graphs obtained in Naya and Niebla for redox potential. While in the generating source (Naya; Fig. 3m), the system has practically no memory in

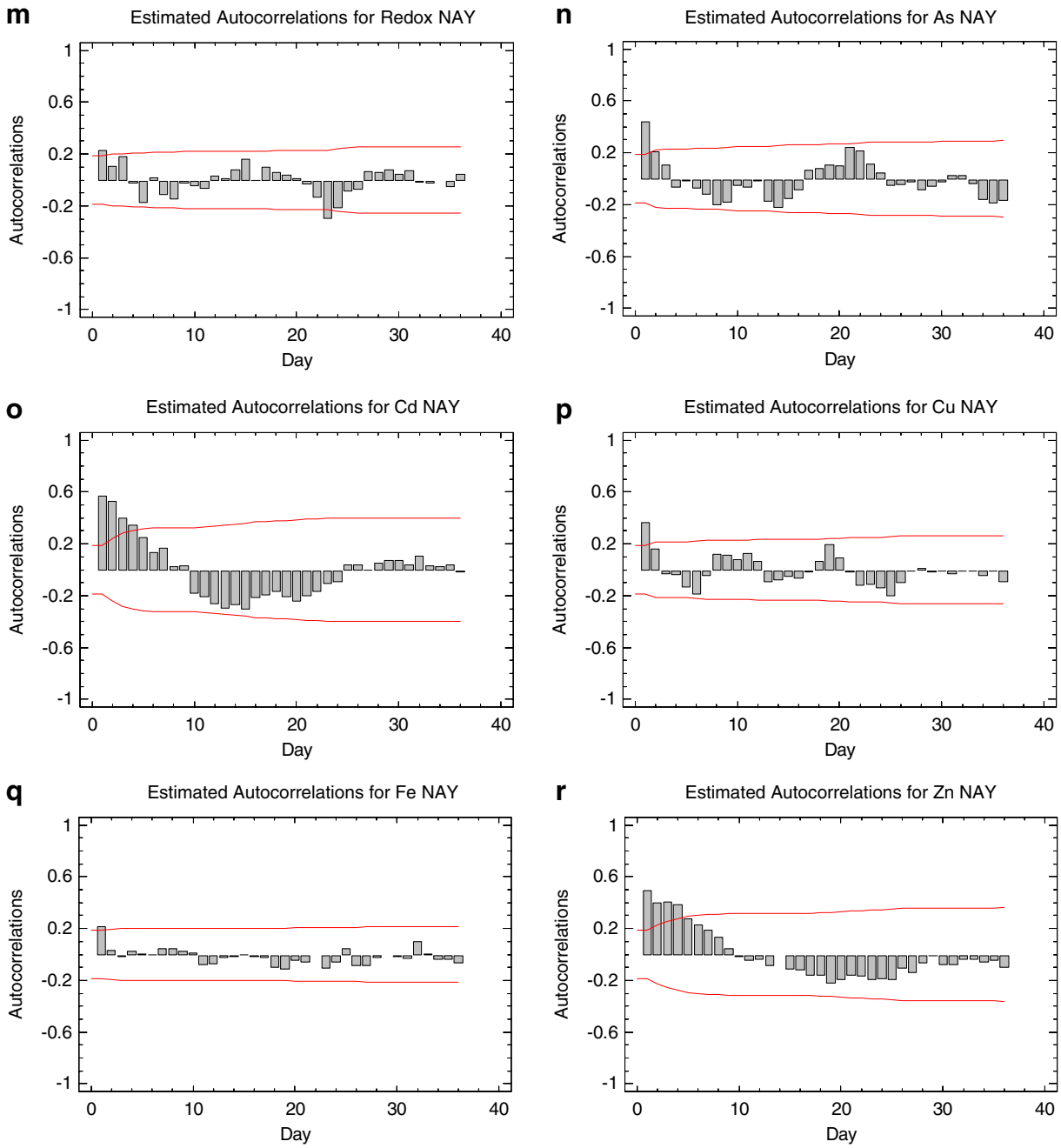

Fig. 3 (continued)

terms of this parameter; in the receiving environment, a graph (Fig. 3c) is obtained which determines an 8-day memory.

The remaining parameters, As, Cu, Fe, and Mn, also display longer memory in the receiving environment; however, for Cd, Zn, and SO_4, the opposite phenomenon is observed. They display longer memory in the generating source (Naya) than in the receiving environment (Niebla).

3.5 Cross-Correlation Functions

No very high cross-correlations were obtained between pairs of the same variables in the generating source and receiving environment. In all cases, certain discreet correlations are observed for almost all cases where t is other than zero (Fig. 4a–j).

In the graph for the estimated cross-correlation of pH in Naya with pH in Niebla (Fig. 4a), negative correlations are detected, with maximums of 0.3, from $t=-20$ to $t=-3$, the time at which the correlation becomes positive with a maximum of 0.2, up to $t=3$, the time at which it becomes negative again.

The graph for conductivity (Fig. 4b) in Naya compared with Niebla displays positive correlations, with maximums of 0.3 from $t=-20$ to $t=0$, the time at which it becomes slightly negative and immediately becomes positive again with a similar value.

Redox potential (Fig. 4c) does not provide a significant cross-correlation graph at the two sites studied. The same is true for Cu, Fe, Zn, and Mn.

In terms of As (Fig. 4d), this reaches a maximum positive correlation of 0.3 for $t=-10$, while at the same time, Cd reaches a negative correlation of −0.5 (the highest of all the crossed parameters).

Sulfates (Fig. 4j) reveal a maximum cross-correlation coefficient of −0.5, for $t=0$.

3.6 Cluster Analysis Graph

A cluster analysis was carried out, entering all the variables obtained from analysis at the two sampling sites, with the aim of trying to find relationships between the parameters from both sites which did not stand out in the previously described analyses. In the graph obtained (Fig. 5) thereafter, two large groups can be described.

A: A group made up of variables, all of them from the generating source, and related to AMD pollution: conductivity, As, SO_4, Fe, Cd, Zn, Mn, Cu. In this group, it is worth pointing out a subgroup including Cd, Zn, and Mn, another subgroup which contains As, SO_4, Cu, and Fe, and another with rainfall and redox and pH of the receiving environment.

B: Another group containing the rest of the variables obtained from the samples taken in the receiving environment (conductivity, Cu, Zn, Mn, Fe, As, Cd, SO_4). It is worth pointing out that this group also contains both the pH and redox potential measured at the generating source. The subgroups obtained in this group are on the one hand Cu, Zn, Mn, Fe, and on the other As, Cd, and furthermore, conductivity, SO_4, and pH and redox potential from Naya.

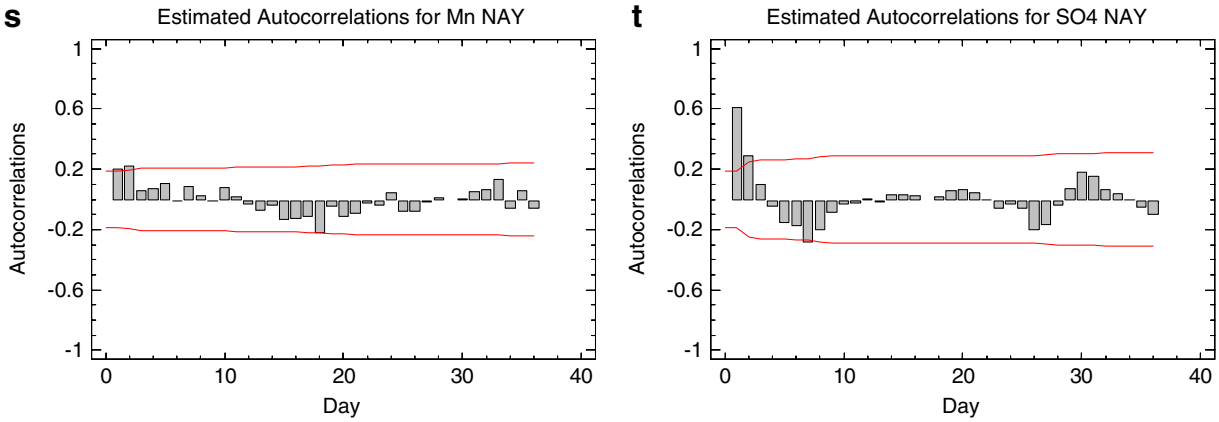

Fig. 3 (continued)

4 Discussion and Conclusions

By studying the results obtained from the statistical processing described above, it can be deduced, first and foremost, that the Tinto River watercourse is highly polluted by acid mine drainage throughout its length. It is also characterized by extremely acidic pH values and high concentrations of heavy metals, As, Cd, and sulfates. More specifically, it can be observed that in spite of its pH being acidic throughout its course, the average and maximum concentrations of dissolved polluting elements are clearly higher in the generating source than in the receiving environment. This is because the high level of pollution starts at this first site, and thereafter, as a result of phenomena involving

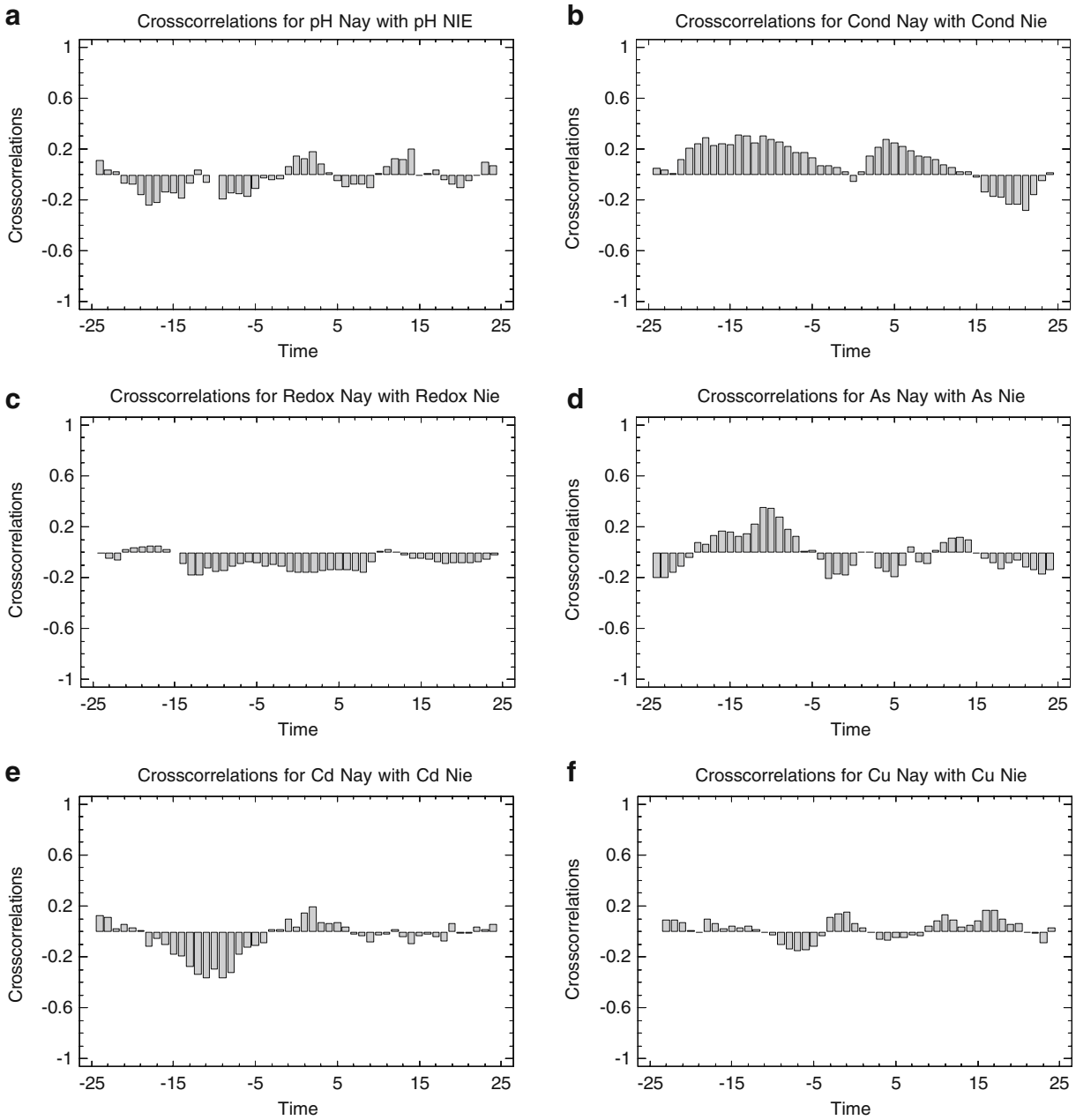

Fig. 4 Graphs showing estimated cross-correlations between the same parameters in the generating source and the receiving environment

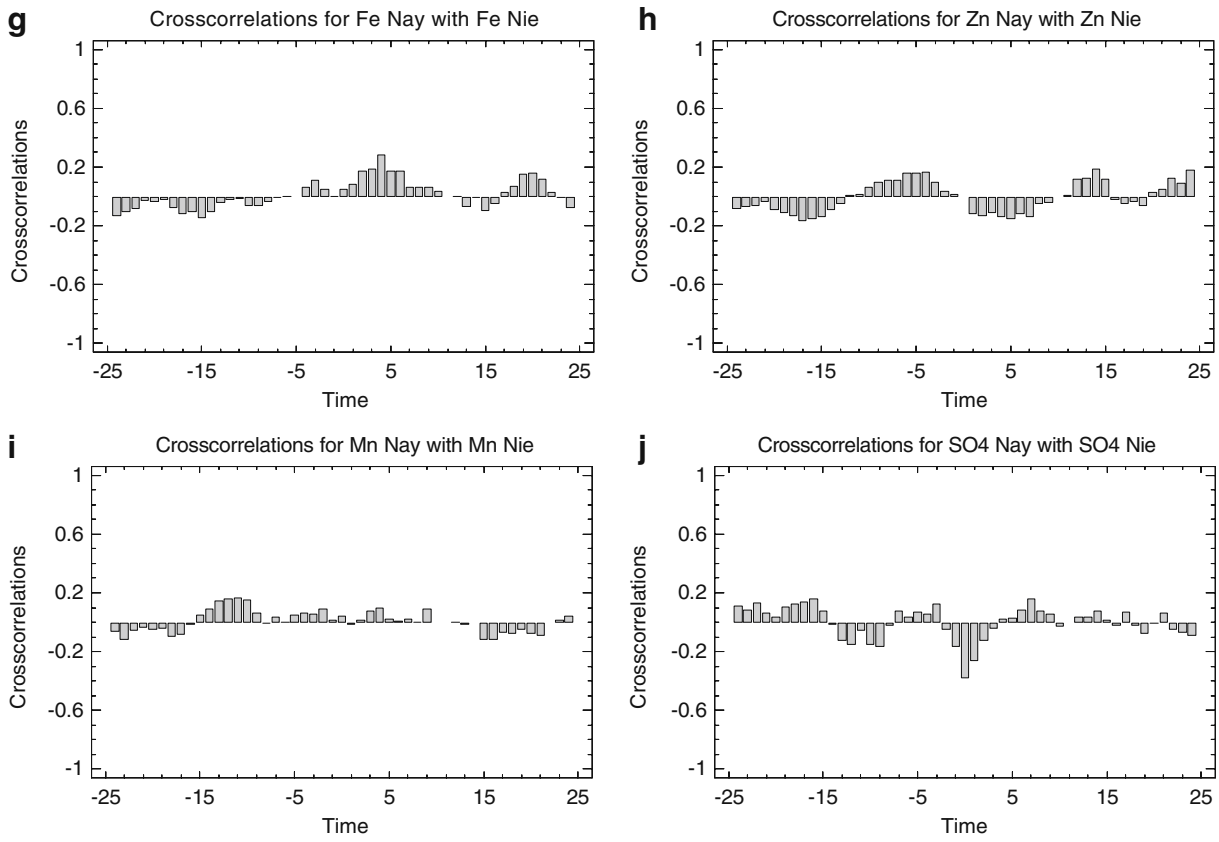

Fig. 4 (continued)

precipitation of Fe oxyhydroxy sulfates and differences in the distribution of rainfall along the river (Cánovas et al. 2008), the metallic load decreases. However, it continues to be high to the end of the river before tidal influence, which modifies the chemistry due to the effect of dilution and the contribution of other elements from the sea.

Specifically and by studying the statistical summary, it can be determined that the order of abundance of the polluting elements, in terms of the concentration of the various parameters in milligrams per liter, follows the pattern below, both in the generating source and the receiving environment:

$$SO4 > Fe > Cu > Zn > Mn > Cd > As$$

which, as can be observed, goes in order of abundance of the elements in pyrite, as described by Ortiz (2003) and indicated in the introduction.

Specifically, attention should be paid to the concentration values for As carried into the river in the generating source, with average values of 640 μg l^{-1} and with a maximum of 1,540 μg l^{-1} (ten times greater than the maximum found in Niebla), which far exceeds 10 μg l^{-1}, the value established by the EU as the maximum permissible

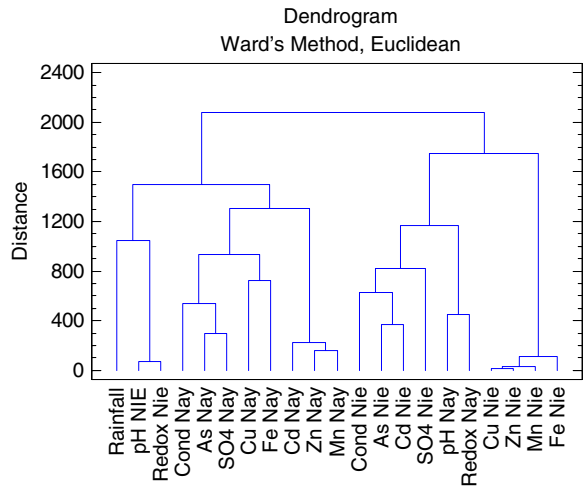

Fig. 5 Cluster analysis graph for all parameters

concentration in drinking water, as a consequence of the high eco-toxicity of this element.

It is also important to point out that the variance of all the parameters is higher in the generating source than in the receiving environment, which indicates greater environmental influence on the water sampled, due to the immediacy with which sulfates dissolve, as determined by the rises and falls in the volume of water due to rain, the contribution from slag heaps, mine tunnels, galleries, etc., which determine greater variability in the individual concentrations of the elements at this site.

Thus, the limited relationship between the variables in the generating source and the receiving environment can be seen from the various statistical processes (correlation matrix, cross-correlation functions, and cluster analysis). Specifically, no correlation was found between the variables from both sites in the correlation matrix. It can only be made out in the cross-correlation function graphs through low correlation, prior to time $t=0$, that pollution in the generating source leads to pollution in the receiving environment.

Acknowledgments The present study was supported by the Andalusian Autonomous Government Excellence Projects, Project P06-RNM-02167.

References

Amils, R. (2006). Rio Tinto as terrestrial analogue for a putative Martian habitat. *AIAA 57th Internacional Astronautical Congreso, IAC, 16*, 11325–11339.

Aroba, J., Grande, J. A., Andujar, J. M., de la Torre, M. L., & Riquelme, J. C. (2007). Application of fuzzy logic and data mining techniques as tool for qualitative interpretation of acid mine drainage processes. *Environmental Geology, 53*, 135–145.

Bisquerra, R. (1989). *Introducción conceptual al análisis multivariable*. Barcelona: Promoc. Public. Univ, S.A.

Borrego, J., Morales, J. A., de la Torre, M. L., & Grande, J. A. (2002). Geochemical characteristics of heavy metal pollution in surface sediments of the Tinto and Odiel river estuary (Southwester Spain). *Environmental Geology, 41*, 785–796.

Cánovas, C. R., Hubbard, C. G., Olías, M., Nieto, J. M., Black, S., & Coleman, M. L. (2008). Hydrochemical variations and contaminant load in the Río Tinto (Spain) during flood events. *Journal of Hydrology, 350*, 25–40.

Casiot, C., Egal, M., Elbaz-Poulichet, F., Bruneel, O., Bancon-Montigny, C., Cordier, M., et al. (2009). Hydrological and geochemical control of metals and arsenic in a Mediterranean river contaminated by acid mine drainage (the Amos River, France): Preliminary assessment of impacts on fish (*Leuciscus cephalus*). *Applied Geochemistry*. doi:10.1016/j.apgeochem.2009.01.006.

Cheng, H., Hu, Y., Luo, J., Xu, B., & Zhao, J. (2008). Geochemical processes controlling fate and transport of arsenic in acid mine drainage (AMD) and natural systems. *Journal of Hazardous Materials*. doi:10.1016/j.jhazmat.2008.10.070.

de la Torre, M. L., Grande, J. A., Jiménez, A., Borrego, J., & Díaz Curiel, J. (2009). Time evolution of an AMD-affected river chemical makeup. *Water Resources Management, 23*, 1275–1289.

Demchack, J., Skousen, J., & McDonald, L. M. (2004). Longevity of acid discharges from underground mines located above the regional water table. *Journal of Environmental Quality, 33*, 656–668.

Egal, M., Elbaz-Poulichet, F., Casiot, C., Motelica-Heino, M., Négrel, P., Bruneel, O., et al. (2008). Iron isotopes in acid mine waters and iron-rich solids from the Tinto–Odiel Basin (Iberian Pyrite Belt, Southwest Spain). *Chemical Geology, 253*, 162–171.

EMCBC. (1996). *The perpetual pollution machine. Acid mine drainage* (pp. 1–6). Canada: B.C. Mining Control.

Fernández-Remolar, D. C., Gómez-Elvira, J., Gómez, F., Sebastián, E., Martín, J., Manfredi, J. A., et al. (2004). The Tinto river, an extreme acidic environment under control iron, as an analog of the Terra Meridiani hematite site of Mars. *Planetary and Space Science, 52*(1–3), 239–248.

Grande, J. A., Borrego, J., de la Torre, M. L., & Sáinz, A. (2003). Application of cluster analysis to the geochemistry zonation of the estuary waters in The Tinto and Odiel rivers. *Environmental Geochemistry and Health, 25*, 233–246.

Grande, J. A., Borrego, J., Morales, J. A., & de la Torre, M. L. (2003). A description of how metal pollution occurs in the Tinto–Odiel rias (Huelva-Spain) through the application of cluster analysis. *Marine Pollution Bulletin, 46*, 475–480.

Grande, J. A., Beltrán, R., Sáinz, A., Santos, J. C., de la Torre, M. L., & Borrego, J. (2005). Acid mine drainage and acid rock drainage processes in the environment of Herrerias Mine (Iberian Pyrite Belt, Huelva- Spain), and impact on the Andevalo dam. *Environmental Geology, 47*, 185–196.

Grande, J. A., Andújar, J. M., Aroba, J., de la Torre, M. L., & Beltrán, R. (2005). Precipitation, pH and metal load in AMD river basins: An application of fuzzy clustering algorithms to the process characterization. *Journal of Environmental Monitoring, 7*, 325–334.

Jiménez, A., Aroba, J., de la Torre, M. L., Andújar, J. M., & Grande, J. A. (2009). Model of behaviour of conductivity versus pH in acid mine drainage waters, based on fuzzy logic and data mining techniques. *Journal of Hydroinformatics, 112*, 147–153.

Lin, C., Wu, Y., Lu, W., Chen, A., & Liu, Y. (2007). Water chemistry and ecotoxicity of an acid mine drainage-affected stream in subtropical China during a major flood event. *Journal of Hazardous Materials, 142*, 199–207.

Morales, J. A., Borrego, J., San Miguel, E. G., López-González, N., & Carro, B. (2008). Sedimentary record of recent tsunamis in the Huelva Estuary (southwestern Spain). *Quaternary Science Reviews, 27*, 734–746.

Nieto, J. M., Sarmiento, A. M., Olías, M., Canovas, C. R., Riba, I., Kalman, J., et al. (2007). Acid mine drainage

pollution in the Tinto and Odiel rivers (Iberian Pyrite Belt, SW Spain) and bioavailability of the transported metals to the Huelva Estuary. *Environment International, 33*(4), 445–455.

Olías, M., Nieto, J. M., Sarmiento, A. M., Cerón, J. C., & Cánovas, C. R. (2004). Seasonal water quality variations in a river affected by acid mine drainage: The Odiel River (South West Spain). *The Science of the Total Environment, 333*, 267–281.

Ortiz M. 2003. *Aproximación a la minería y metalurgia de minas de Riotinto desde la antigüedad al siglo XIX.* PhD Thesis. Spain.

Pinedo Vara, I. (1963). *Piritas de Huelva*. Madrid: Summa.

Ruiz, F., Borrego, J., González-Regalado, M. L., López, N., & Carro, B. (2008). Abad M. Impact of millennial mining activities on sediments and microfauna on the Tinto River estuary (SW Spain). *Marine Pollution Bulletin, 56*, 1258–1264.

Sáez, R., Pascual, E., Toscano, M., & Almodovar, G. R. (1999). The Iberian type of volcano-sedimentary massive sulphide deposits. *Mineralium Deposita, 34*, 549–570.

Sáinz, A., Grande, J. A., de la Torre, M. L., & Sánchez-Rodas, D. (2002). Characterisation of sequential leachate discharges of mining waste rock dumps in the Tinto and Odiel rivers. *Journal of Environmental Management, 64*, 345–353.

Sáinz, A., Grande, J. A., & de la Torre, M. L. (2004). Characterisation of heavy metal discharge into the Ria of Huelva. *Environment International, 30*, 557–566.

Sáinz, A., Grande, J. A., & de la Torre, M. L. (2005). Application of systemic approach to the study of pollution of the Tinto and Odiel rivers (Spain). *Environmental Monitoring and Assessment, 102*, 435–445.

Sánchez-Rodas, D., Gómez-Ariza, J. L., Giraldez, I., Velasco, A., & Morales, E. (2005). Arsenic speciation in river and estuarine waters from southwest Spain. *The Science of the Total Environment, 345*(1–3), 207–217.

Sarmiento, A. M., Nieto, J. M., Casiot, C., Elbaz-Poulichet, F., & Egal, M. (2009). Inorganic arsenic speciation at river basin scales: The Tinto and Odiel Rivers in the Iberian Pyrite Belt, SW Spain. *Environmental Pollution, 157*(4), 1202–1209.

Sarmiento, A. M., Nieto, J. M., Olías, M., & Cánovas, C. R. (2009). Hydrochemical characteristics and seasonal influence on pollution by acid mine drainage in the Odiel river basin. *Applied Geochemistry*. doi:10.1016/j.apgeochem.2008.12.025.

Sobron, P., Rull, F., Sobron, F., Sanz, A., Medina, J., & Nielsen, C. J. (2007). Raman spectroscopy of the system iron(III)–sulfuric acid–water: An approach to Tinto River´s (Spain) hydrogeochemistry. *Spectrochimica Acta Part A, 68*, 1138–1142.

Stoker, C. R., Cannon, H. N., Duganan, S. E., Lemke, L. G., Glass, B. J., Miller, D., et al. (2008). The 2005 MARTE robotic drilling experiment in Río Tinto, Spain: Objectives, approach, and results of a simulated mission to search for life in the martian subsurface. *Astrobiology, 8*(5), 921–945.

Vicente-Martorell, J. J., Galindo-Riaño, M. D., & García-Vargas, M. (2009). Bioavailability of heavy metals monitoring water, sediments and fish species from a polluted estuary. *Journal of Hazardous Materials, 162*, 823–836.